Ground state and infrared response of triple concentric quantum ring structures

José María Escartín, Manuel Barranco, and Martí Pi[*]
Departament d'Estructura i Constituents de la Matèria, Facultat de Física,
and IN²UB, Universitat de Barcelona, Diagonal 647, 08028 Barcelona, Spain

Within local-spin density-functional theory, we study the ground state and infrared response of two-dimensional, triple concentric quantum ring nanostructures. Changes in their physical properties are presented as a function of the number of electrons or the intensity of a perpendicularly applied magnetic field. We discuss the addition spectrum of few-electron triple quantum rings at zero magnetic field, as well as the physical appearance of the ground state and dipole response of selected systems containing up to 50 electrons. We also investigate the ground state, persistent currents, and charge- and spin-density responses of a system made of 30 electrons.

I. INTRODUCTION

Since the first quantum rings of nanoscopic size were fabricated,[1–3] these fascinating systems have drawn a considerable attention due to the interest in studying physical phenomena that take place in such nonsimply connected devices, such as the Aharonov-Bohm effect[4–7] and the appearance of persistent currents.[8] As quantum dots, quantum rings can be coupled forming "artificial ring molecules."[9,10] Theoretical studies on double quantum rings coupled vertically[11–14] and laterally[15,16] have discussed the molecular properties of these systems.

Quantum rings may also be coupled concentrically. Double concentric quantum rings have been experimentally realized,[17,18] and a series of recent works have addressed their ground-state (gs) properties[19–24] and far-infrared (FIR) response, see Refs. 25 and 26, and references therein. It has been shown that the radial distribution of the electrons within the system depends on several parameters. Indeed, at zero magnetic field the location of the particles in the inner or in the outer ring is decided from the competition between the centrifugal and Coulomb energy terms—favoring the population of the larger one—with the confining potential contribution.[19] The presence of a perpendicularly applied magnetic field gives rise to the well-known diamagnetic and Zeeman orbital terms that compete with the above-mentioned ones, favoring, respectively, the occupation of the inner and the outer ring.[21] Interestingly, in the low-density regime, i.e., when the Coulomb interaction becomes dominant, in addition to such radial localization among the inner and outer rings, the electrons can show angular localization in the intrinsic reference frame of the system, giving rise to "crystallized configurations" often referred to as "Wigner molecules"[27,28] since they are reminiscent of the well-known Wigner crystallization occurring in the two-dimensional electron gas.

Experimentally, it has been shown that the electronic radial distribution in double concentric quantum rings (DCQRs) can be inferred from transport measurements via the variation in the period of the Aharonov-Bohm effect associated to the changes in the enclosed magnetic flux.[29] Also, it should be observable in the FIR response of these systems.[26]

Very recently, GaAs/AlGaAs multiple—from triple to quintuple—concentric quantum ring structures have been fabricated by droplet epitaxy techniques and characterized by reflection high-energy electron-diffraction and atomic force microscopy techniques.[30] Motivated by this work, we have employed the local-spin density-functional theory (LSDFT), also termed LSDA, to anticipate some properties of the ground state and the dipole response of strictly two-dimensional triple concentric QRs (TCQRs).

This paper is organized as follows. In Sec. II we briefly introduce the theoretical model and the formalism we have employed to describe TCQR. In Sec. III we discuss the addition spectrum of few-electron TCQR as well as the physical appearance of the gs and dipole response of several systems containing up to $N=50$ electrons at zero magnetic field. We also study in detail the gs, persistent currents and spin- and charge-density dipole response as a function of the intensity of a $N=30$ TCQR submitted to a perpendicular magnetic field B, whose variation has clear effects on the electronic distribution of the particles within the constituent rings and allows to find different, radially localized electron configurations. Finally, our conclusions are drawn in Sec. IV.

II. THEORETICAL MODEL

It is technically feasible to represent TCQR by three-dimensional models, incorporating the cross-section profile of the device and the conduction-band offset between different semiconductor components to build the electron confining potential. This has been done for double concentric quantum rings in the noninteracting electron case,[31] and could be extended to the interacting case using the LSDFT for obtaining their gs (Ref. 32) and the time-dependent LSDFT for obtaining their dipole response.[33] This is numerically very costly for several tens of electrons, especially if one has to carry out systematic calculations.

Other methods also aiming at realistically describing the lateral confinement have been applied to the case of single-electron quantum rings[34] but their extension to the many electron case is unclear. Besides, these approaches have serious difficulties to work out the dipole response of quantum ring structures, so they have been only used to determine

ground-state properties or single-electron spectra. For these reasons, we have opted for using here a simpler two-dimensional representation for the TCQR which includes the basic ingredients for the physical description of these systems, especially since the constituent rings are coupled in plane and their shape is very flat (they are less than 5nm thick).

Since experimental multiple rings exhibit a high degree of circular symmetry, we have represented them by a circularly symmetric confining potential composed of three overlapping parabolae with frequencies ω_1, ω_2, and ω_3 and vertices at radii R_1, R_2, and R_3 $(R_1 < R_2 < R_3)$, respectively,

$$V_{\text{conf}}(r) = \frac{m}{2}\min\{\omega_k^2(r-R_k)^2\}_{k=1,2,3}. \quad (1)$$

The rings are formed at a disorder-free GaAs/AlGaAs heterostructure containing electrons with effective mass $m^* = 0.067$, i.e., $m = m^* m_e$, being m_e the electron mass, dielectric constant $\epsilon = 12.4$, and effective gyromagnetic constant $g^* = -0.44$. The TCQR may be submitted to a perpendicular magnetic field B pointing toward the positive z axis. While the values for the radii, namely, $R_1 = 40$ nm, $R_2 = 70$ nm, and $R_3 = 105$ nm, have been taken from one of the experimental devices,[30] the frequencies have been fixed rather arbitrarily to $\omega_1 = 34$ meV, $\omega_2 = 35$ meV, and $\omega_3 = 36$ meV. Large frequencies are imposed to produce the strong confinement felt by the TCQR, and the condition $\omega_1 < \omega_2 < \omega_3$ aims at compensating to some extent the geometric effect of the radius on the effective surface of the constituents rings, as otherwise most electrons would sit at the outer ring and the system would unpurposely behave as one single quantum ring. With our choice for the frequencies, the constituent rings are in a weak Coulomb coupling rather that in a strong quantum-mechanical coupling regime. This seems the more interesting regime, as the use of small frequencies to model the TCQR confinement would result in too a large coupling between the rings, that would effectively behave as one single thick quantum ring whose characteristics have been described in the past.[35] Note also that the reduced size of the TCQR justifies avoiding the consideration of impurities in the nanostructure.

The gs of the N-electron system is obtained through the solution of the Kohn-Sham (KS) equations for the single-particle (sp) wave functions $\varphi_{n\ell\sigma}(\mathbf{r})$. Assuming circular symmetry, the KS equations, in so-called "dot units" $(\hbar = e^2/\epsilon = m = 1)$ read

$$\left[-\frac{1}{2}\left(\frac{\partial^2}{\partial r^2} + \frac{1}{r}\frac{\partial}{\partial r} - \frac{\ell^2}{r^2}\right) - \frac{\omega_c}{2}\ell + \frac{1}{8}\omega_c^2 r^2 + V_{\text{conf}}(r) + V_H + V_{\text{xc}} \right.$$

$$\left. + \left(W_{\text{xc}} + \frac{1}{2}g^*\mu_B B\right)\eta_\sigma \right] u_{n\ell\sigma}(r) = \varepsilon_{n\ell\sigma}u_{n\ell\sigma}(r), \quad (2)$$

where $V_H = \int d\mathbf{r}' \rho(\mathbf{r}')/|\mathbf{r}-\mathbf{r}'|$ is the Hartree potential, $V_{\text{xc}} = \partial\mathcal{E}_{\text{xc}}(\rho,\xi)/\partial\rho|_{\text{gs}}$ and $W_{\text{xc}} = \partial\mathcal{E}_{\text{xc}}(\rho,\xi)/\partial\xi|_{\text{gs}}$ are the variations in the exchange-correlation energy density $\mathcal{E}_{\text{xc}}(\rho,\xi)$ in the local approximation taken at the gs, and $\rho(r)$ and $\xi(r)$ are the electron and spin magnetization densities. The exchange-correlation energy density $\mathcal{E}_{\text{xc}}$ has been constructed from the results of the unpolarized and fully polarized two-

dimensional electron gas[36] in the same way as in Ref. 37. In the above equation, $\omega_c = eB/(mc)$ is the cyclotron frequency and $\mu_B = e\hbar/(2m_e c)$ is the Bohr magneton, and $\eta_\sigma = +1$ (-1) for $\sigma = \uparrow$ $(\downarrow)$. The vector potential has been chosen in the symmetric gauge, namely, $\mathbf{A} = B(-y,x,0)/2 = Br\hat{\mathbf{e}}_\theta/2$, where $\hat{\mathbf{e}}_\theta$ is the unit vector in the direction of the azimuthal coordinate θ. The sp states are of the form $\varphi_{n\ell\sigma}(\mathbf{r}) = u_{n\ell\sigma}(r)e^{-i\ell\theta}\chi_\sigma$ with $n = 0, 1, 2, \ldots$ being the principal quantum number (number of radial nodes), and $\ell = 0, \pm1, \pm2, \ldots, -\ell$ being the projection of the sp orbital angular momentum on the z axis.

Our theoretical model imposes circular symmetry in the nanostructures and our computational method does so to the considered physical states. This treatment thus allows the localization of electrons within each of the constituent rings but forbids their azimuthal localization within them. Such azimuthal localizations are sometimes found within LSDFT,[27] and there is a vast literature, see, e.g., Refs. 27 and 28, and references therein, discussing whether or not they are artifacts of mean-field theory. For double concentric quantum rings, we have found that sometimes these localizations correlate well with the physical ones appearing in the exact two-body density of the system,[24] thus revealing the internal symmetry of the ground state. Unfortunately, there is no way to tell if it is physical or not but carrying out an exact calculation, which is unaffordable for more than a few electrons.

Calculations have been carried out at a small but nonzero temperature T of 0.5 K or smaller. On the one hand, this represents better the actual physical situation. On the other hand, the structure of the sp spectrum discussed in Sec. III shows that there are sp levels near to the Fermi level localized in different rings, but with sp energies very close. As a consequence, they have a fractional (thermal) occupation. In this sense, the constituent rings are not only strictly Coulomb coupled. The thermal occupation probabilities f_α are determined by the Fermi-Dirac distribution and the normalization condition $N = \Sigma_\alpha f_\alpha$, which fix the chemical potential. The gs electron number density is $\rho(r) = \Sigma_\alpha f_\alpha |u_\alpha(r)|^2$ [normalized such that $\int\rho(r)d^2\mathbf{r} = N$] while the gs spin magnetization density is expressed in terms of the spin of sp state α, σ_α^z, as $m(r) = \Sigma_\alpha f_\alpha \sigma_\alpha^z |u_\alpha(r)|^2$.

The dipole strength functions $S(\omega)$ have been determined within linear-response theory. This implies to obtain first the correlation function in the spin and density channels in the local-spin density-functional theory. Once the correlation functions have been obtained, one determines the response functions, whose imaginary parts are proportional to the strength functions. We refer the reader to Ref. 38 for a detailed presentation of the method.

III. RESULTS AND DISCUSSION

A. $B=0$ case

We have computed the structure of the $N=1$ to 12 TCQR at $T=0.1$ K. The electron distribution among the three rings is collected in Table I. We have carefully checked that these configurations are the lowest energy ones by starting the KS minimization from more than one initial guess, which is crucial in view of the nonsimply connected topology arising

TABLE I. Electron number distribution at $T=0.1$ K among the three concentric rings for $N=1-13$.

N	1	2	3	4	5	6	7	8	9	10	11	12	13
R_1	1			1	1	1.3	1.5	1.7	2	2.2	2.4	2.7	1
R_2		2	3	3									3
R_3					4	4.7	5.5	6.3	7	7.8	8.6	9.3	9

from the TCQR confining potential. In all cases, the total orbital angular momentum has been found to be $L_z=0$, while the total spin on the z axis, S_z, is maximum in most cases. For $N=2$, this is a spurious effect of the LSDFT—at zero magnetic field it can be rigorously proved that the gs is a spin singlet—that can be fixed by including self-interaction corrections.[39] In our case, we have also checked that breaking the circular symmetry, in Cartesian coordinates, yields a singlet gs which corresponds to one electron in the R_1 ring and another in the R_3 ring, whose energy is sensibly that of the axially symmetric, triplet configuration used to draw Fig. 3. The tendency of the system to have a sizeable spin polarization, also found, e.g., for single quantum rings[6,27] and some few-electron double concentric quantum rings,[23] is due to its large size, which makes the electron system very dilute, thus favoring exchange and correlation effects that tend to spin polarize the TCQR in accordance with a general property of the two-dimensional electron gas.[36,40] We want to point out that LSDA enhances this physical effect, as it overestimates the exchange-correlation energy by a few percent as compared, e.g., with diffusion Monte Carlo calculations.[23] Besides, treating the system as strictly two-dimensional also magnifies Coulomb exchange effects, irrespective of the theoretical framework the system is described within.[41] We have checked in some cases that the difference between the fully polarized and unpolarized configurations is fairly small, see also Ref. 23.

The electron rearrangements shown in the Table I are a clear indication of the nontrivial contribution of the Coulomb, confinement, and centrifugal energy terms, whose balance eventually produces the TCQR ground state. It also shows that the system has to host more than about ten electrons to allow for a real interplay between the three constituents rings. This of course depends on the confining potential we are using, but let us stress that the confinement produced by the TCQR synthesis process is rather strong, and hence one would expect that the rings are in the capacitive coupling regime addressed in this work. That number of electrons renders more justified the use of LSDFT to address the TCQR gs and somewhat unavoidable to obtain its dipole spectrum.

We show in Fig. 1 the electron-density distribution $\rho(r)$ and spin magnetization $m(r)$ for $N=20$, together with the confining potential $V_{\text{conf}}(r)$. It is worth stressing that the sp orbitals are remarkably localized in either ring, and that the fractional electron occupation of some of them is not due to the sharing of an orbital by two rings, but rather to the fractional occupation of two different orbitals of very similar sp energy and different orbital angular momentum, each peaked in a different ring.

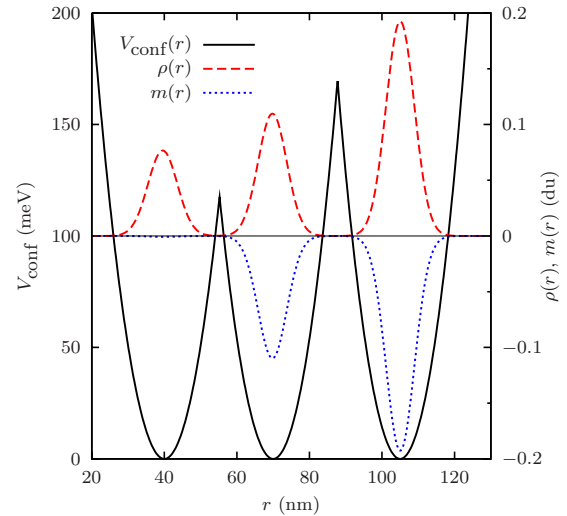Figure 1 also shows that the inner ring is unpolarized whereas the other two are fully polarized. "Mixed phase"

FIG. 1. (Color online) The solid line displays the TCQR confining potential (meV) as a function of the radial distance r (nm). The electron density $\rho(r)$ (dashed line) and the spin magnetization $m(r)$ (dotted line) in dot units are also shown for $N=20$ at $B=0$ and $T=0.1$ K.

configurations have been reported in two-dimensional quantum dots described within an unrestricted Hartree-Fock approach,[42] where the presence of an impurity produced an uneven electronic-density distribution, in which some regions of the N-electron system behave like a Fermi liquid (unpolarized system) while, simultaneously, other more dilute regions display the typical quasiclassical Wigner distribution of the charge maxima in the electron-density profile. Since our system is circularly symmetric, the latter phase is substituted here by the full polarized one.

The low-energy sp spectrum of the $N=20$ TCQR at 0.1 K is shown in Fig. 2. It is easy to determine which ring each sp state belongs to since they turn out to be peaked in either of the three constituent rings. This is presented in the corresponding panels of this figure. We stress that the three rings are coupled and have a common chemical potential.

It may be interesting to ascertain the influence of these rearrangements on two observable quantities, namely, the addition spectrum and the infrared response. Figure 3 shows the addition energies, defined as

$$\Delta_2(N) = E(N+1) - 2E(N) + E(N-1), \qquad (3)$$

where $E(N)$ is the total energy of the N-electron TCQR. The addition spectrum shows some departures from the conspicuous even-odd structure found in the case of a single quantum ring.[43,44]

Figure 4 shows the low-energy charge and spin strength functions $S(\omega)$ for $N=10$, 20, 30, 40, and 50 TCQR as a function of the excitation energy (meV) at $B=0$ and $T=0.5$ K. The intensities are fixed in such a way that for a given N, the more intense peaks in each channel roughly have the same height. These peaks arise from electron-hole pairs that have the same principal quantum number n. It can be seen in the panels corresponding to $N=30$, 40, and 50 how the spin response (dashed lines) is redshifted with re-
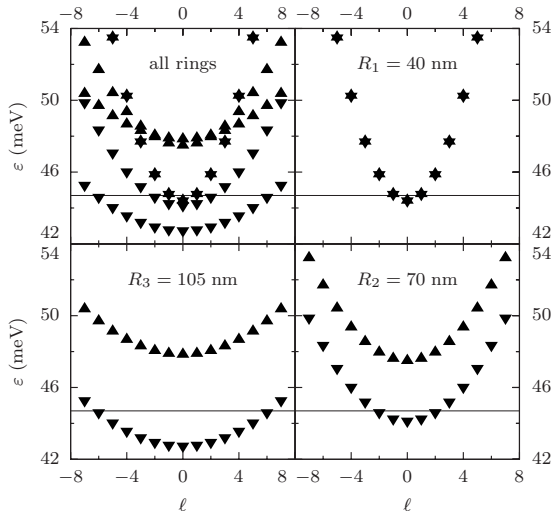
FIG. 2. Top left panel: single-particle energies as a function of *minus* the sp orbital angular momentum ℓ for the $N=20$ TCQR at $B=0$ and $T=0.1$ K. Up (down) triangles represent spin-up (down) states. The horizontal thin solid line is the chemical potential. From the top right panel, clockwise, the other three panels represent the same sp energies split into the three constituent rings R_1, R_2, and R_3.

spect to the free response (dotted line), whereas the charge response (solid line) is blueshifted. This is because the electron-hole interaction is attractive and weak in the spin channel while it is strong and repulsive in the density channel. This seems to be violated for the $N=10$ and 20 TCQR, but these two systems are full—or nearly—spin polarized, and in this case the spin- and charge-density responses coincide. Some low-intensity peaks are located at very high energies, e.g., in the 34–36 meV energy range for $N=30$ and contribute very little to the strength. These high-energy peaks arise from electron-hole pairs differing in the principal quantum number by $\Delta n \geq 1$.

Note that as the rings are capacitively coupled, the response cannot be obtained, even approximately, as the sum of the responses of each ring hosting the number of electrons previously determined by solving the KS equations for the
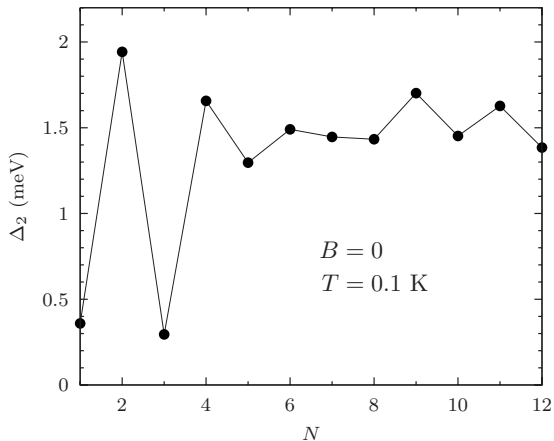

FIG. 3. Addition energy Δ_2 (meV) at $T=0.1$ K as a function of N for $N=1–12$. The lines have been drawn as a guide to the eyes.
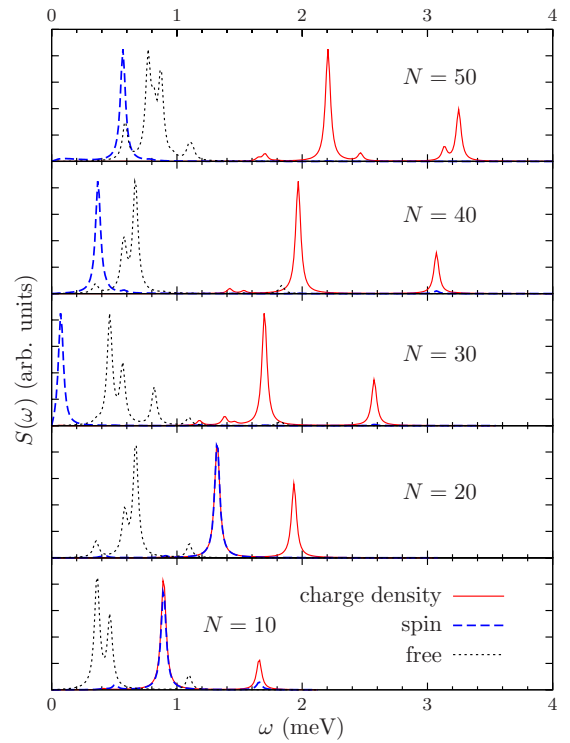

FIG. 4. (Color online) Charge dipole strength (solid lines, arbitrary units), spin dipole strength (dashed lines, arbitrary units), and free-particle dipole strength (dotted lines, arbitrary units) for TCQR with $N=10$, 20, 30, 40, and 50 electrons as a function of the excitation energy (meV) at $B=0$ and $T=0.5$ K. The scales are fixed in such a way that, for a given N, the most intense peaks of all channels roughly have the same height.

TCQR. However, it is possible to roughly infer the origin of the main peaks in the charge-density response displayed in Fig. 4 by correlating the number of electrons in a selected ring with the contribution of a given peak to the f-sum rule, which on the one hand equals the electron number N divided by 2, and on the other hand can be expressed as an integral of $S(\omega)$ weighted with ω.[38,45]

A more sensible way of determining the contribution of a given ring to the spin- and charge-density responses is to isolate the sp orbitals confined into that ring, and build out of them the free response and the electron-hole interaction without considering the contribution from the other sp states. The rationale of this method is easy to understand recalling the structure of the Dyson-type integral equation obeyed by the LSDFT correlation function $\chi_{\sigma\sigma'}$ in terms of the free-particle spin-density correlation function $\chi_{\sigma\sigma'}^{(0)}$,

$$\chi_{\sigma\sigma'}(\mathbf{r},\mathbf{r}';\omega) = \chi_{\sigma\sigma'}^{(0)}(\mathbf{r},\mathbf{r}';\omega) + \sum_{\sigma_1\sigma_2} \int d\mathbf{r}_1 d\mathbf{r}_2$$
$$\times \chi_{\sigma\sigma_1}^{(0)}(\mathbf{r},\mathbf{r}_1;\omega) K_{\sigma_1\sigma_2}(\mathbf{r}_1,\mathbf{r}_2) \chi_{\sigma_2\sigma'}(\mathbf{r}_2,\mathbf{r}';\omega),$$
$$(4)$$

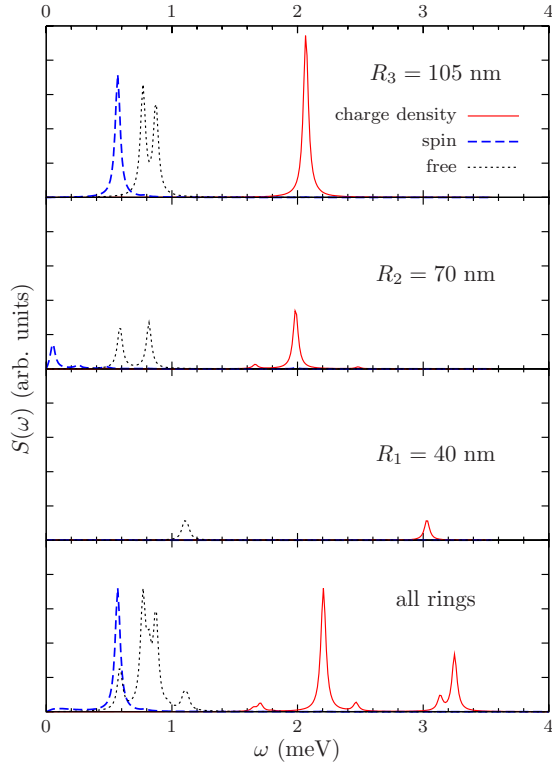where the kernel $K_{\sigma\sigma'}(\mathbf{r},\mathbf{r}')$ is the two-body interaction,

FIG. 5. (Color online) Bottom panel: charge dipole strength (solid lines), spin dipole strength (dashed lines), and free-particle dipole strength (dotted lines) for a TCQR with $N=50$ at $B=0$, $T=0.5$ K. The other panels display the strengths arising from the R_i rings, obtained as indicated in the text. The scales are the same for every channel in all panels, and they are fixed in the bottom panel, so that the most intense peaks of each channel display roughly the same height. The very different strengths of the channels in the different panels can be explained from the f-sum rules of the corresponding operators and (sub)system since the f-sum rules are proportional to the number of electrons hosted.

$$K_{\sigma\sigma'}(\mathbf{r}_1,\mathbf{r}_2) = \frac{1}{|\mathbf{r}_1 - \mathbf{r}_2|} + \left.\frac{\partial^2 \mathcal{E}_{xc}(\rho,\xi)}{\partial\rho_\sigma \, \partial\rho_{\sigma'}}\right|_{gs} \delta(\mathbf{r}_1 - \mathbf{r}_2) \quad (5)$$

and the free-particle spin-density correlation function at finite temperature $\chi^{(0)}_{\sigma\sigma'}(\mathbf{r},\mathbf{r}';\omega)$ is obtained from the KS sp wave functions, energies, and occupation probabilities as

$$\chi^{(0)}_{\sigma\sigma'}(\mathbf{r},\mathbf{r}',\omega) = -\delta_{\sigma,\sigma'}\sum_{\alpha\beta} \varphi_\alpha^*(\mathbf{r})\varphi_\beta(\mathbf{r})\frac{f_\alpha - f_\beta}{\varepsilon_\alpha - \varepsilon_\beta + \omega + i\eta}$$

$$\times \varphi_\beta^*(\mathbf{r}')\varphi_\alpha(\mathbf{r}'), \quad (6)$$

where the label α (β) refers to a sp level with spin σ (σ') and occupation probability f_α (f_β).

Note from the above equations that, since the exchange-correlation contribution to $K_{\sigma\sigma'}(\mathbf{r}_1,\mathbf{r}_2)$ is proportional to a Dirac delta, this procedure disentangles the strength in the spin-density channel, but it does strictly not in the charge-density channel because the Coulomb interaction is long range. In spite of this, the method has allowed us to identify the highest-energy peak in Fig. 4 with the charge-density mode from the R_1 ring, and the most intense peak with the
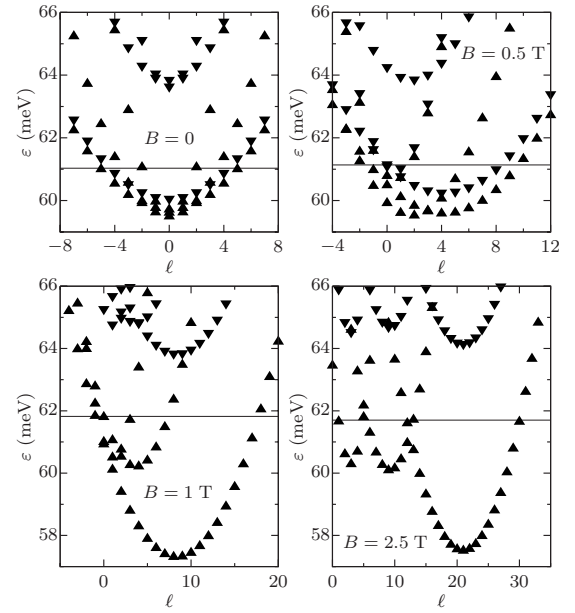

FIG. 6. Single-particle energies as a function of minus the sp orbital angular momentum ℓ for the $N=30$ TCQR at $T=0.5$ K and selected B values: 0, 0.5, 1, and 2.5 T. Up (down) triangles represent spin-up (down) states. Horizontal, thin solid lines are displayed at the energies of the respective chemical potentials.

charge-density mode of the R_3 ring. The charge-density response of the R_2 ring is still entangled with that of the R_3 ring because both responses are in the same energy range, although that arising from the R_3 ring dominates, since it is more populated.

A detailed example of strength disentangling is presented in Fig. 5 for $N=50$ at $B=0$ and $T=0.5$ K. The number of electrons hosted in each ring is ~ 6 for R_1, ~ 12 for R_2, and ~ 32 for R_3. Inspection of this figure shows that the main peaks of the spin-density response of a given ring R_k are not drifted, whereas those of the charge-density response present some drift because of the Coulomb coupling with electrons sitting in the other rings.

Figure 4 also shows that the energy of the charge-density peaks increases as N does. We recall that Kohn's theorem does not hold for ringlike confinements. The effect is difficult to establish quantitatively, as the number of electrons in each ring and their local spin magnetization vary as a function of N in a nontrivial way.

Finally, the spin-density response is dominated by a low-energy peak also arising from the R_3 ring. This peak is very soft in the $N=30$ case. Soft peaks are also present for $N=40$ and 50, but carry very little strength, see, e.g., the low-energy structure in the spin channel for $N=50$ coming from contributions of the R_1 and R_2 rings, as displayed in Fig. 4.

B. $B\neq 0$ case

The low-energy sp spectrum of the $N=30$ TCQR at 0.5 K and B values from 0 to 2.5 T is shown in Fig. 6. As B increases, sp states appear distributed into different parabolae, so that sp states within each of the parabolae lie within
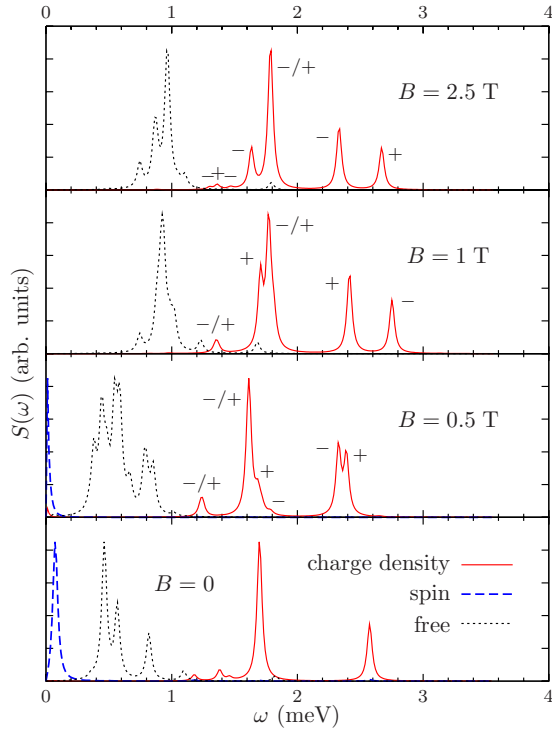
FIG. 7. (Color online) Low-energy charge (solid lines, arbitrary units) and spin dipole strength (dashed lines, arbitrary units) for $N=30$ at $T=0.5$ K as a function of the excitation energy (meV). The scales are fixed in such a way that, for a given B, the most intense peaks in all channels roughly have the same height. The (+) and (−) symbols near the main charge-density peaks indicate their circular polarization. Some structures are superpositions of peaks with different polarizations; they are denoted by the compound symbol (−/+), since in all cases the (−) polarization is the dominant one, eventually.

the same ring, thus recovering the known characteristic behavior of single quantum rings.[35] Furthermore, the parabolae are more open the larger the radius is, and when B increases they are displaced toward increasing ℓ's, the larger the radius the faster the displacement. Within this range of magnetic fields, the system displays different polarizations without any regular dependence on B, with a big tendency to be fully polarized, as is to be expected from LSDA computations at relatively low densities. When the system is not completely polarized, one or two of the constituent rings may be completely polarized, the remaining ones being nearly paramagnetic. Accurate observation of the systematics shows that the middle ring is the easiest one to polarize (see, e.g., the $B=0.5$ T panel of Fig. 6) while the outer ring is the hardest one to polarize. Finally, for $B \gtrsim 2.5$ T, the system is always fully polarized. These intricate changes in the ground-state structure produce nontrivial changes in the dipole response and the permanent currents as a function of B.

Figure 7 shows the charge and spin strength functions for $N=30$ at $T=0.5$ K and selected B values. The intensities are fixed as in Fig. 4. In the absence of magnetic field, the peaks corresponding to positive and negative circular polarizations are degenerate. This degeneracy is lifted when $B \neq 0$, and for one single quantum ring the splitting would increase as B

does. In the TCQR, this trend is partially lost because the electron content and polarization of each of the rings also change with B, and one may see how the splitting beats as a function of B. For the same reason, the charge-density response also experiences nonmonotonous changes.

In FIR spectroscopy polarization of light is a tunable degree of freedom of the incident electromagnetic radiation and circular polarization control of terahertz radiation has been reported, e.g., in Ref. 46. Therefore, peaks corresponding to different circular polarizations—experimental channels—could be independently addressed experimentally. However, the splitting of the dipole mode corresponding to different circular polarizartions at low B fields is rather small, the energy distance between them clearly smaller than 1 meV. Therefore, depending on the dispersion of shapes of the TCQR (and the consequent width of the peaks), and given the present experimental precision of FIR spectroscopy, it is possible that their energies may not be experimentally differentiable.

The spin-density response is still dominated by a soft, low-energy peak. It is also worth noting that in some cases the charge and spin responses are strongly coupled, indicating that some charge-density peaks are seen in the spin channel and vice versa. This coupling has also been found in quantum dots[38] and metal clusters.[47,48]

We have determined the persistent current in the TCQR, whose intensity is calculated as $I=-e\int dr\mathbf{J}(r)\cdot\hat{\mathbf{e}}_\theta$, where $\mathbf{J}$ is the probability current density vector consisting of a paramagnetic plus a diamagnetic term, $\mathbf{J}=\mathbf{J}_\mathrm{p}+\mathbf{J}_\mathrm{d}$ with

$$\mathbf{J}_\mathrm{p} = -\frac{\hbar}{m}\hat{\mathbf{e}}_\theta\frac{1}{r}\sum_\alpha f_\alpha\ell_\alpha|u_\alpha(r)|^2,$$

$$\mathbf{J}_\mathrm{d} = \frac{e}{mc}\rho(r)\mathbf{A} = \frac{eB}{2mc}r\rho(r)\hat{\mathbf{e}}_\theta \qquad (7)$$

in the present gauge. Thus, since the diamagnetic current can be integrated analytically, the total intensity is $I=-e\int dr\mathbf{J}_\mathrm{p}(r)\cdot\hat{\mathbf{e}}_\theta-e^2BN/(4\pi mc)$. It is worth noting that both contributions have opposite signs and there is a large cancellation between both currents.

Figure 8 displays the intensity corresponding to the persistent current as a function of the applied magnetic field. It displays oscillations due to changes in the TCQR ground state induced by the applied magnetic field.[13,14,43,44] The behavior is slightly more regular for $B \gtrsim 2.5$ T since there are no polarization changes within that range. However, current jumps due to both changes in the electron occupation of the constituent rings and changes of the occupied sp angular momenta within each ring are present in all the studied range of magnetic fields.

In order to have a better insight of the intricate oscillations of the LSDA intensities, we have compared them for magnetic fields B at which the system only displays completely polarized LSDA ground states with those of a simpler model, namely, a system of independent spinless electrons that move within three uncoupled one-dimensional rings with the same radii R_k ($k=1,2,3$) at respective offset potentials V_k, and at the same finite temperature than before,
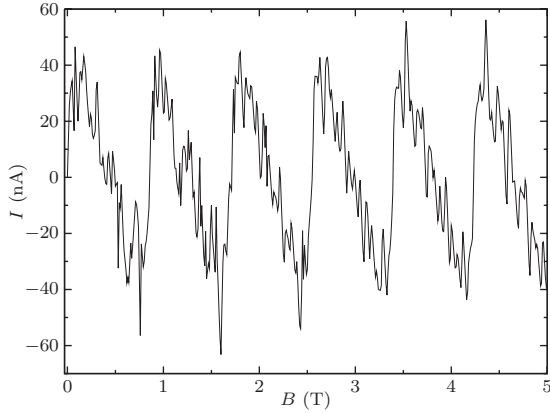
FIG. 8. Intensity of the persistent current of the TCQR as a function of the applied magnetic field, computed using the LSDA. The intensity starts from zero in the absence of magnetic field and displays main oscillations with amplitudes of $\Delta B \simeq 0.85$ T.

$T = 0.5$ K. Any eigenstate of the corresponding single-particle Hamiltonian can be labeled using two quantum numbers $|k, \ell\rangle$: the index of the ring where it lies k and again the opposite of the projection of the sp orbital angular momentum on the z axis ℓ. The energy of the sp state $|k, \ell\rangle$ is

$$\varepsilon_{k\ell} = \frac{\hbar^2}{2mR_k^2}\left(\ell - \frac{\Phi_k}{\Phi_0}\right)^2 + V_k \tag{8}$$

and the intensity of the current that it generates is

$$I_{k\ell} = \frac{\hbar e}{2\pi mR_k^2}\left(\ell - \frac{\Phi_k}{\Phi_0}\right), \tag{9}$$

where $\Phi_k = \pi R_k^2 B$ is the magnetic flux through the kth ring and $\Phi_0 = hc/e$ is the quantum of flux. In order to build the multiparticle ground state, the sp states $|k, \ell\rangle$ are filled, with respective occupations $f_{k\ell}$, following the Fermi-Dirac distribution at the given temperature. The V_k offsets thus control to some extent the total occupations of each of the rings.

Figure 9 displays the intensities of the persistent currents of the system for this independent-particle model with $V_1 = V_2 = 0$ and $V_3 = -3$ meV. We have chosen these offsets as a first-order approximation to reproduce the behavior displayed by the single-particle Kohn-Sham eigenvalues of the polarized systems shown in Fig. 6, where the different Coulomb and exchange-correlation contributions lead to a minimum of the outer ring parabola significantly lower than those of the other single-ring parabolae.[49]

Oscillations in B have a ring-dependent characteristic period of $\Delta B_k = \Phi_0/(\pi R_k^2)$, so they are faster the larger the radius of the ring is. The period in B of the main oscillations ($\Delta B_1 \simeq 0.82$ T), due to the change of the occupied levels within the inner ring, is in good agreement with that resulting from the LSDA calculation. Minor oscillations in the single-ring current intensities are due to changes in the occupation of the rings, i.e., electron jumps between rings. The oscillations of the total intensity are a superposition of the oscillations of the single-ring intensities, in correspondence with the nondominant oscillations of the intensities resulting from the LSDA calculation. Finally, we just recall that the main
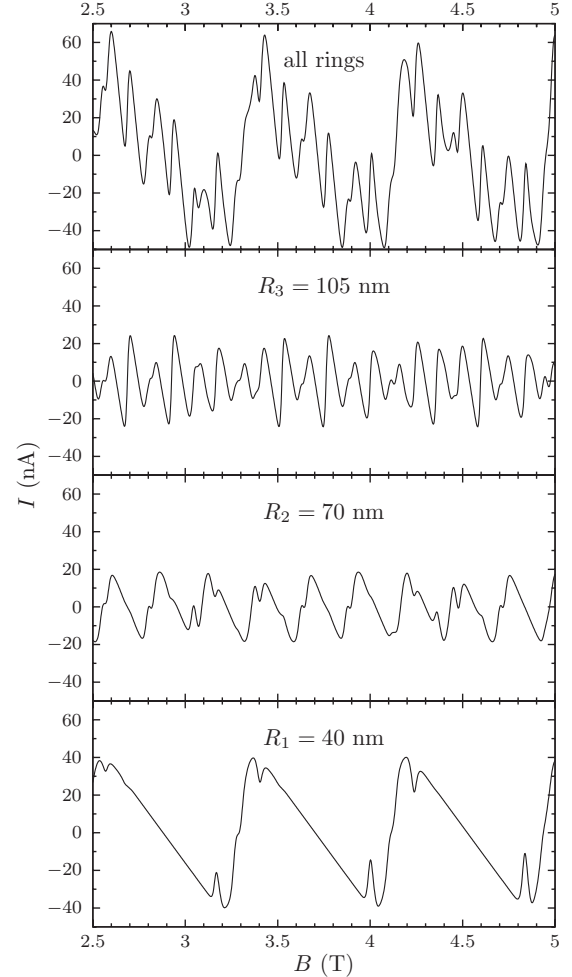

FIG. 9. Intensity of the persistent currents of the system (top panel) and each of the constituting rings (rest of panels) for the independent particle model of one-dimensional rings. The oscillations of the total current are dominated by that of the inner ring.

effect of the finite temperature is a smoothing of the level transitions and thus of the current oscillations.

It should be stressed that the combination of oscillations with intrinsically different magnetic field periodicities, both in the independent particle model and in the LSDA calculation, is a direct consequence of the coupling of constituent rings of different sizes. Vertically coupled nanoscopic rings are formed by rings with similar radii and thus do not display this effect.[13,14]

IV. SUMMARY

We have addressed, in the local spin-density approximation, the ground state and infrared response of triple concentric quantum ring structures capacitively coupled. Within this coupling limit, electrons are radially localized in the constituent rings. Depending on the total number of electrons, some of the rings are fully polarized, whereas others are not. This manifests, e.g., in the dipole response of the system, and in the coupling of the density and spin responses, as previously found for quantum dots and metal nanoparticles.

Changes induced by a perpendicular magnetic field in the total angular momentum and in the distribution of the electrons among the rings have been disclosed. In particular, the *B* dispersion of the dipole modes becomes nonmonotonous, presenting some beats. Similarly, the persistent current displays main oscillations, a characteristic feature of a single quantum ring, whose period is associated with the geometric extent of the smallest ring, modulated by others arising from those pertaining to the larger rings, due either to the change in their number of electrons, or to the evolution of the angular momentum as a function of *B*. The combination of intensity oscillations with different magnetic field periodicities is a consequence of the coupling of rings with different radii.

Both effects arise from the nonconnected topology of these devices, so it might well be that these effects also show up in double concentric rings. We expect them to be more marked for TCQR than for DCQR, as they are manifestations of the filling in of the constituent rings when the number of electrons increases, or of the electron jumping from a constituent ring to another caused by an applied magnetic field. Clearly, their appearance critically depends on the way the TCQR has been made, as confinement plays a substantial role in determining which coupling regime—Coulombic or quantal—the actual system is in. Our calculations just show how some TCQR experimental observables are influenced in the most likely regime these systems are synthesized, namely, the weak Coulomb coupling regime, and might help characterize them.

ACKNOWLEDGMENTS

*marti@ecm.ub.es

[1] J. M. García, G. Medeiros-Ribeiro, K. Schmidt, T. Ngo, J. L. Feng, A. Lorke, J. Kotthaus, and P. M. Petroff, Appl. Phys. Lett. **71**, 2014 (1997).

[2] A. Lorke and R. J. Luyken, Physica B **256-258**, 424 (1998).

[3] A. Lorke, R. J. Luyken, A. O. Govorov, J. P. Kotthaus, J. M. Garcia, and P. M. Petroff, Phys. Rev. Lett. **84**, 2223 (2000).

[4] T. Chakraborty and P. Pietiläinen, Phys. Rev. B **50**, 8460 (1994).

[5] U. F. Keyser, C. Fühner, S. Borck, R. J. Haug, M. Bichler, G. Abstreiter, and W. Wegscheider, Phys. Rev. Lett. **90**, 196601 (2003).

[6] S. Viefers, P. Koskinen, P. S. Deo, and M. Manninen, Physica E **21**, 1 (2004).

[7] P. Offermans, P. M. Koenraad, J. H. Wolter, D. Granados, J. M. García, V. M. Fomin, V. N. Gladilin, and J. T. Devreese, Appl. Phys. Lett. **87**, 131902 (2005).

[8] N. A. J. M. Kleemans, I. M. A. Bominaar-Silkens, V. M. Fomin, V. N. Gladilin, D. Granados, A. G. Taboada, J. M. García, P. Offermans, U. Zeitler, P. C. M. Christianen, J. C. Maan, J. T. Devreese, and P. M. Koenraad, Phys. Rev. Lett. **99**, 146808 (2007).

[9] F. Suárez, D. Granados, M. L. Dotor, and J. M. García, Nanotechnology **15**, S126 (2004).

[10] D. Granados, J. M. García, T. Ben, and S. I. Molina, Appl. Phys. Lett. **86**, 071918 (2005).

[11] L. G. G. V. Dias da Silva, J. M. Villas-Bôas, and S. E. Ulloa, Phys. Rev. B **76**, 155306 (2007).

[12] M. Royo, F. Malet, M. Barranco, M. Pi, and J. Planelles, Phys. Rev. B **78**, 165308 (2008).

[13] L. K. Castelano, G.-Q. Hai, B. Partoens, and F. M. Peeters, Phys. Rev. B **78**, 195315 (2008).

[14] L. K. Castelano, G.-Q. Hai, B. Partoens, and F. M. Peeters, J. Appl. Phys. **106**, 073702 (2009).

[15] J. Planelles, F. Rajadell, J. I. Climente, M. Royo, and J. L. Movilla, J. Phys.: Conf. Ser. **61**, 936 (2007).

[16] T. Chwiej and B. Szafran, Phys. Rev. B **78**, 245306 (2008).

[17] T. Mano, T. Kuroda, S. Sanguinetti, T. Ochiai, T. Tateno, J. Kim, T. Noda, M. Kawabe, K. Sakoda, G. Kido, and N. Koguchi, Nano Lett. **5**, 425 (2005).

[18] T. Kuroda, T. Mano, T. Ochiai, S. Sanguinetti, K. Sakoda, G. Kido, and N. Koguchi, Phys. Rev. B **72**, 205301 (2005).

[19] J. I. Climente, J. Planelles, M. Barranco, F. Malet, and M. Pi, Phys. Rev. B **73**, 235327 (2006).

[20] G. Fuster, M. Pacheco, and Z. Barticevic, Braz. J. Phys. **34**, 666 (2004).

[21] B. Szafran and F. M. Peeters, Phys. Rev. B **72**, 155316 (2005).

[22] F. J. Culchac, N. Porras-Montenegro, and A. Latgé, J. Phys.: Condens. Matter **20**, 285215 (2008).

[23] L. Colletti, F. Malet, M. Pi, and F. Pederiva, Phys. Rev. B **79**, 125315 (2009).

[24] J. M. Escartín, F. Malet, M. Barranco, and M. Pi, Physica E **42**, 841 (2010).

[25] J. M. Escartín, F. Malet, A. Emperador, and M. Pi, Phys. Rev. B **79**, 245317 (2009).

[26] J. M. Escartín, F. Malet, M. Pi, and M. Barranco, Phys. Status Solidi C **7**, 2608 (2010).

[27] S. M. Reimann and M. Manninen, Rev. Mod. Phys. **74**, 1283 (2002).

[28] C. Yannouleas and U. Landman, Rep. Prog. Phys. **70**, 2067 (2007).

[29] A. Mühle, W. Wegscheider, and R. J. Haug, Appl. Phys. Lett. **91**, 133116 (2007).

[30] C. Somaschini, S. Bietti, N. Koguchi, and S. Sanguinetti, Nano Lett. **9**, 3419 (2009).

[31] J. Planelles and J. I. Climente, Eur. Phys. J. B **48**, 65 (2005).

[32] F. Ancilotto, D. G. Austing, M. Barranco, R. Mayol, K. Muraki, M. Pi, S. Sasaki, and S. Tarucha, Phys. Rev. B **67**, 205311 (2003).

[33] M. Pi, F. Ancilotto, E. Lipparini, and R. Mayol, Physica E **24**, 297 (2004).

[34] V. M. Fomin, V. N. Gladilin, S. N. Klimin, J. T. Devreese, N. A. J. M. Kleemans, and P. M. Koenraad, Phys. Rev. B **76**, 235320 (2007).

[35] A. Emperador, M. Barranco, E. Lipparini, M. Pi, and Ll. Serra,

Phys. Rev. B **59**, 15301 (1999).

[36] B. Tanatar and D. M. Ceperley, Phys. Rev. B **39**, 5005 (1989).

[37] M. Koskinen, M. Manninen, and S. M. Reimann, Phys. Rev. Lett. **79**, 1389 (1997).

[38] Ll. Serra, M. Barranco, A. Emperador, M. Pi, and E. Lipparini, Phys. Rev. B **59**, 15290 (1999).

[39] M. Pi, A. Emperador, M. Barranco, and F. Garcias, Phys. Rev. B **63**, 115316 (2001).

[40] C. Attaccalite, S. Moroni, P. Gori-Giorgi, and G. B. Bachelet, Phys. Rev. Lett. **88**, 256601 (2002); **91**, 109902(E) (2003).

[41] M. Rontani, F. Rossi, F. Manghi, and E. Molinari, Appl. Phys. Lett. **72**, 957 (1998).

[42] C. Yannouleas and U. Landman, Phys. Rev. B **61**, 15895 (2000).

[43] A. Emperador, M. Pi, M. Barranco, and E. Lipparini, Phys. Rev. B **64**, 155304 (2001).

[44] J. C. Lin and G. Y. Guo, Phys. Rev. B **65**, 035304 (2001).

[45] E. Lipparini, *Modern Many-Particle Physics: Atomic Gases, Quantum Dots and Quantum Fluids*, 2nd ed. (World Scientific, Singapore, 2008).

[46] R. Shimano, H. Nishimura, and T. Sato, Jpn. J. Appl. Phys., Part 2 **44**, L676 (2005).

[47] M. B. Torres and L. C. Balbás, J. Phys.: Condens. Matter **12**, 4365 (2000).

[48] Y. Yin, P.-A. Hervieux, R. A. Jalabert, G. Manfredi, E. Maurat, and D. Weinmann, Phys. Rev. B **80**, 115416 (2009).

[49] A. Emperador, F. Pederiva, and E. Lipparini, Phys. Rev. B **68**, 115312 (2003).